Journal of Molecular Graphics and Modelling 29 (2011) 1006–1014

Contents lists available at ScienceDirect

Journal of Molecular Graphics and Modelling

journal homepage: www.elsevier.com/locate/JMGM

Inter-ring rotation of apolipoprotein A-I protein monomers for the double-belt model using biased molecular dynamics

Thomas R. Caulfield*

School of Chemistry and Biochemistry, Georgia Institute of Technology, Atlanta, GA 30332-0230, United States

ARTICLE INFO

Article history:
Received 23 June 2010
Received in revised form 29 March 2011
Accepted 19 April 2011
Available online 27 April 2011

Keywords:
Apolipoprotein A-I
Discoidal high density lipoprotein
HDL
Double belt model
Paris mutant
Milano mutant
Simulation

ABSTRACT

The double belt model for lipid-bound discoidal apolipoprotein A-I consists of two alpha-helical monomers bound about an unilamellar bilayer of lipids. Previous work, based on salt bridge calculations, has demonstrated that the L5/5 registration, Milano mutant, and Paris mutant are preferred conformations for apolipoprotein A-I. The salt bridge scoring indicated better *energetic* scoring in these alignments. The Paris (R151C) and Milano (R173C) mutants indicate a mode of change must be available. To find proper registration, one proposed change is a 'rotationally' independent circular motion of the two protein monomers about the lipid unilamellar bilayer core. Here, we present computational data for independent inter-ring rotation of the two alpha-helical monomers about the lipid unilamellar bilayer core. The simulations presented here support the existing double-belt model. We find the rotation of the two protein monomers is able to occur with biasing. We determine that a cysteine mutant at Glu107 as a possible target for future mutational studies. Since HDL remodeling is necessary for cholesterol transport, our model for remodeling through dynamics has substantial biomedical implications.

1. Introduction

Apolipoprotein-AI (Apo A-I) plays a critical role in the maintenance of cholesterol molecules in mammalian organisms [1]. Apo A-I is the major protein component of antiatherogenic high-density lipoprotein (HDL). ApoA-I is a protein biomolecule and it is usually associated with other lipophilic molecules (such as phospholipids and cholesterol) in supramolecular assemblies (e.g. lipoproteins of just one type, namely HDL) [2,3]. ApoA-I participates in the reverse transport of cholesterol from tissues to the liver for excretion by promoting cholesterol efflux from tissues and by acting as a cofactor for the lecithin cholesterol acyltransferase (LCAT). ApoA-I is a major protein of plasma HDL, and ApoA-I is also found in chylomicrons. ApoA-I is synthesized in the liver and small intestine [4,5]. This vital mechanism of lipid transport and cholesterol recycling is important for the biosynthesis of new molecules, the proper maintenance of cellular functions in higher organisms, and reduced risk for atherosclerosis [6–8]. Apo A-I is the integral component of both the spheroidal and discoidal (hockey puck-shape) nascent HDL particle.

1.1. Apolipoprotein A-I's double belt-model structural arrangement

Various models for Apo A-I have been described in the literature [9–11]. All models found in the literature are being refined with experiments and molecular modeling. An attractive instance is the double belt model, which has been previously noted in the literature [9]. We obtained the model for the Apo A-I double belt model from Harvey and Segrest (personal communication). This model consists of two basic protein sequences running in antiparallel directions with an alpha-helical orientation. The N-terminal domain consists of residues 1–43, while the lipid binding C-terminal domain consists of residues 44–243 (or, in another model, 44–247). The N-terminal domain has been postulated to be either globular or helical, however recent experimental work using AFM and CD supports a random-coil globular structure in a lipid free environment and a helical state in a lipid-mimicking detergent [12]. A previous model for the smallest discoidal HDL has been postulated and confirmed [9–11]. This double belt model was shown to consist of about 160 lipids sequestered into a small unilamellar bilayer within the circular double belt [9]. The arrangement of the two chains is such that the proteins form circular rings around a bundle of lipids. The structure of the belt consists of two ampipathic α-helix protein chains. Apo A-I's α-helix forms 3.67 residues per turn, contains a hydrophobic surface facing the lipids, and has an optimal geometry to form intermolecular salt bridge interactions with an antiparallel arrangement that matches the lipid free

* Corresponding author. Tel.: +1 404 275 3684; fax: +1 404 385 4499.
E-mail address: thomas.caulfield@chemistry.gatech.edu

1093-3263/$ – see front matter © 2011 Elsevier Inc. All rights reserved.
doi:10.1016/j.jmgm.2011.04.005

crystal structure [13]. Each protein α-helix contains eight 22-mer and two 11-mer tandem amino acid sequence repeats. The periodicities of the two monomers of apo A-I are punctuated by prolines, which aid in maintaining the circular geometry [14]. Previous work supports a preference for the double belt model, but is still debated [15].

Binding of the apo A-I to lipid in the discoidal HDL particle for the belt conformation is driven by non-specific hydrophobic interactions, and interhelical salt bridging plays a key role in determining the specificity of helix–helix registration. Prior evidence for the belt model using molecular dynamics and HDL and POPC lipids supports interhelical registration with the use of a helical wheel [16]. While previous molecular dynamics experiments have profiled lipid behavior under varying conditions [17]. Interhelical salt bridges determine the preference for one antiparallel interface and dictate the registration of the helices [18–21], where the maximal salt bridging model corresponded to the alignment found in the apo Δ(1–43) A-I crystal structure [13].

1.2. Apo A-I Paris and Milan mutants and disease

Apo A-I is also known to be involved in some interesting diseases. Particularly, there is a mutation that occurs where the apo A-I arginine residue is mutated into a cysteine. The Milan mutation consists of the apoA-I_{Milano} mutation at residue 173, while the Paris mutation consists of the apoA-I_{Paris} mutation at residue 151 [22–24]. Additionally, the wild-type apo A-I lacks the cysteine residues within its genetic sequence [22]. Interestingly, the arginine to cysteine mutation does not appear to hamper the reconstituted mutant HDL particles, and both the wild-type HDL particles and the mutant HDL particles have a comparable capacity to clear dimyristoylphosphatidylcholine (DMPC) emulsions and promote normal cholesterol efflux [25–27]. Amongst populations of persons with either the Paris and Milano mutation, there exist decreased levels of HDL, but paradoxically also a reduced risk for atherosclerosis [22,23,26].

ApoA-I_{Milano} reconstitutes into HDL particles, with either two or four distinct molecules of apoA-I, forming in two possible diameters. The size of these reconstituted HDL particles is similar in size to wild-type apo A-I HDL particles [24,25]. While the apoA-I_{Paris} HDL particles can form into particles with three possible diameters [28].

Different helical registrations for models of apo A-I have been examined for interaction energies between the helix–helix side chains of the two protein monomers of the double belt model [29]. Previously, it has been hypothesized a mode of re-assigning the registrations may be possible, thus allowing shifts between registrations after the discoidal complex is formed. It is not clear from experimental work what the mechanism for different registrations forming. It is known for the Milano and Paris-type mutants, apo A-I forms a disulfide bond between the cysteine residues, thus locking the protein monomers together. If different registrations for Paris and Milano variants were to form after initial synthesis, then protein monomer mobility would be necessary to find alternate registrations.

Based upon the belt model for apo A-I and the Paris and Milano models published previously [15,24], we have simulated a viable model for the independent rotation of the two protein monomers. Using wild-type apoA-I, we construct a molecular dynamics simulation over a 360° rotation of the two monomers. Exploring each registration along this path, the interaction energy is plotted, revealing an inherent stability in the Paris and Milano mutants from salt bridge interactions. We define four other low energy states, three of which are lower in energy than the Paris and Milano mutants. The methods section outlines our choice of model and arrangement.

2. Methods

2.1. Molecular modeling

The belt model for apo A-I was previously published was used as a starting structure [14,15]. Initial modeling was carried out with INSIGHT and the Quanta package on an SGI workstation [30]. Subsequent modeling was carried out using VMD for molecular setup [31]. Simulations were carried out using NAMD [32,33]. We utilized the well-known and previously published models from the Harvey and Segrest Labs [29,34–37]. This initial study serves as a launching point for future studies on heterodimers and alternative orientations.

2.2. Simulation methodology

Each simulation system consisted of a periodic box containing the Apolipoprotein A-I protein, 176 molecules of POPC lipids in a bilayer, and solvent molecules, for a total of 151,000 atoms. We added two Na^+ counterions to neutralize the simulation cell, and then added sufficient Na^+ and Cl^- ions replicating a physiological solution. In the random initial placement of ions, a minimum distance of 10 Å between the ions was maintained, and the ions were placed in bulk water and away from the protein. A typical simulation cell is visible in supplemental materials (Movie S1). The apoA-I protein plus POPC lipid bilayer was fully solvated using TIP3P water molecules in a box of dimensions 164 Å × 160 Å × 115 Å [38]. The periodic cells were designed that the minimum distance between the molecules and the edge of the water box was 20 Å. Our results indicate that the apo A-I and POPC residues do not interact with the edge at edge-to-edge distances >35 Å, thus we expect the size of the cell is sufficient to prevent interaction between molecules in neighboring cells. Two Na^+ ions were added to balance the charge of the terminal protein residues, and then sodium and chloride ions were added, yielding electric neutrality in the unit cells. Simulations were run using a constant number of particle, volume, and temperature conditions and all used periodic boundary conditions. Simulations were run in NAMD using the CHARMM27 parameter set with a time step of 2 fs using SHAKE [32,39,40]. Electrostatics interactions were calculated using the particle-mesh Ewald method [41]. Nonbonded interactions had a real-space cutoff of 15 Å. The systems were minimized 4000 steps of steepest decent with the apo A-I/POPC complex held fixed, then subsequently, for an additional 4000 steps of the adopted-basis Newton-Raphson method with decreasing harmonic restraints on the apo A-I/POPC complex. Each system was then equilibrated for 100 ps with the apo A-I/POPC complex fixed with a harmonic restraint of 0.5 kcal/mol applied to the heavy atoms of apo A-I and POPC, so that only solvent and ions were free to move. Each system was then equilibrated for another 150 ps with the temperature coupling to a heat bath of 310 K under constant volume conditions with gradually relaxing restraints, 0.5 kcal/mol/Å^2 to 0.25 kcal/mol/Å^2 to 0.13 kcal/mol/Å^2 (50 ps each), and then under constant volume conditions with no restraints for 100 ps [42,43]. The simulation temperature was kept constant using the Berendsen algorithm by weakly (τ_p = 0.1 ps) coupling the protein, lipid, and solvent to a temperature bath of 310 K [44]. Likewise, the pressure was kept constant by isotropically coupling the system to a pressure bath of 1 bar, with a coupling constant of τ_p = 2 ps and a compressibility of 4.5×10^{-5} bar^{-1}. Restrained equilibration runs were done for 5 ns to ensure the system stability, while low restraint k < 1 kcal/mol was applied at Cα atoms to maintain the original starting structure for production runs under Maxwell's demon molecular dynamics (MdMDs) runs [45]. MdMD has been previously described in the literature [45]. Here we present the use of the MdMD method for sampling rare conformational pathways by removing entropy from the system (Fig. S2).

Table S1 outlines the various MdMD schemes used for sampling with MD intervals called *MDsprints*. Fig. S2 shows a schematic for the MdMD algorithm, which has been previously discussed [45].

2.3. Maxwell's demon molecular dynamics

Briefly, the MdMD method repeated scans a direction of conformations using short intervals of MD called "MDsprints", where at the end of each sprint the "demon" measures the system for a global property, in this case, the relative position of the two protein monomers along the *Z*-axis, such that we are aiming for *z*-angle increasing for each monomer relative to the other. The MDsprint may be anywhere from 50 femtoseconds to 10 picoseconds. If the measure property has satisfied the Maxwellian demon (score) with an incremental increase, decrease, or other measurable property, like the amount of rotation measured relative to the two protein monomers, then the MDsprint is maintained in an archive file, whilst if the sprint is a failure, then it is annulled and the system restarts from the last archived state. From the last archived state, the system may be reinitialized for velocities upon the waters (stp) derived from a Boltzman distribution of the system. This is a "randomizer" for the MDsprints.

Total simulation time amongst all runs, including disregarded states of sampling, would be >1 μs of MD sampling. However, the archived success states for all conformations that move incrementally forward based on the biasing scheme totals approximately 100 ns. In the case of parallel motion between the two protein monomers, successful rotations were completed in 3 ns of MdMD, which corresponds to over 300 ns of total MD time with a 1 percent success rate. Likewise, for the 30 ns rotations achieved using MdMD, over 800 ns of MD time with 2–4 percent success rate on each run. In all simulations that utilized our Maxwell's demon biasing algorithm [45,46], a structure from the previous state's run was used to start each successive run. Coordinates were saved between 2 and 40 ps intervals.

Biasing forces are applied with a constant force of 20 pN as shown in Fig. 2. This force is only applied as a projection onto the *X*–*Y* plane relative to the *Z*-axis of rotation, which is defined by the center of the apo A-I protein monomers ring-like structure. This force is applied at n and $n+7C\alpha$ atoms. Additionally, the constant force-biasing algorithm may be coupled with all other atoms to sample conformational space during the course of the simulation. With the subset of biasing on Cα's, we utilized an iterative and adaptive algorithm called Maxwell's demon (MdMD) (Movie S2). MdMD utilizes intervals of MD ranging from 50 fs to 10 ps in duration. After each interval, a global variable is measured, measuring parameters of the system. This method has been previously reported [46]. MdMD was done with a size-optimizing search for the best time-length interval for optimal sampling (Fig. 2).

The biggest limitation to any MdMD study is the length of time for desired transition to occur. In the longer MdMD simulations (30 ns runs), we lowered our TCL-forces applied from C_n to C_{n+7}, which were mapped onto the *XY*-plane (to remove any *Z*-axis unraveling). The criterion for success was made more lenient to allow for larger MDsprints (time between scoring up to 10 ps) before assessing with the demon. For both the mutant (Glu107Cys) and native sequence, the 3-ns MdMD run archive (contains all of the cumulative successes), a non-planar, non-idealized model results. The structure for the apolipoprotein from MdMD more closely matches the shapes described in the literature [47]. However, bear in mind the 3-ns cumulative-MdMD run is approximately 300 ns of conformational landscape sampled in the direction of the reaction coordinate that results in a 180° rotation of apolipoprotein monomer 1 (ring 1) relative to apolipoprotein monomer 2 (ring 2). Likewise, there is a 180° rotation for ring 2 relative to ring 1 occurs, thus giving the appearance of 360° rotation. Supplemental Table S1 contains the specific details of simulations. Additionally, we did native and mutant simulations for very slow rotational sampling with a net result of around 25–30 ns of successful MDsprints, which corresponds to over 800 ns of sampling time. A mutation of Glu107 to Cys107 was modeling in using the VMD plug-in [31]. Results from the Glu107 energy profile (see results) indicated testing Cys107 for indicated mutational studies. As described above, minimization, equilibration, production and MdMD biasing were conducted on the mutant to achieve similar results. Both a short run and a long MdMD biasing run were conducted on the Glu107Cys mutant.

3. Results and discussion

3.1. Ring rotation

Here, we present the data for independent inter-ring rotation of the two alpha-helical monomers about the unilamellar bilayer contained within the core. We find that the rotation of the two protein monomers in a 'forward' anti-parallel direction is able to occur with MdMD biasing (Supplemental Movie S1 and Movie S2). Additionally, the biasing force applied in this scheme (20 pN per *n*, $n+7C\alpha$) is shown in Fig. 2. Whereas, the time for the forward direction occurs in approximately 3 ns, the reverse direction requires approximately 4.5 ns and has more disorder in inter-protein side chain interactions.

3.2. Independent 'Ring Rotation'

Fig. 1A is a continuous series of snapshots from the idealized simulation of the discoidal apo A-I protein/POPC lipid complex (3.4 ns MdMD run time). In the series of snapshots the time is indicated in the lower left corner. At frame 1 time = 0 ns, we can see a detailed molecular belt model for apolipoprotein A-I in discoidal high density lipoprotein. In frame 2 time = 0 ns, the lipids (gray) is removed visually to show both protein monomers of apo A-I (red and blue). As well, two large VdW representations of residues in the chains are shown, so that motion is indicated. In frame 3 time = 0 ns, some of the core lipids (yellow) are visually reintroduced to illustrate the relative stability of lipids for the simulation. In frame 4 time = 0.5 ns, the initial motion of the two monomers is evident and the lipid core is preserved. In frame 5 time = 1.0 ns to frame 9 time = 3.0 ns, we see the movement of the two rings about the *Z*-axis. Lastly, in frame 10, time = 3.0 ns, the lipids are redrawn to show any conformational change. Supplemental Movie S1 shows the idealized ring rotation.

Fig. 1B is a continuous series of snapshots from both the native sequence and mutant sequence of the discoidal apo A-I protein/POPC lipid complex (3.4 ns MdMD run time). A series of snapshots reveals the global conformational changes and 360° ring rotation as indicated by the reference molecule shown on each monomer as a large green sphere. The native sequence simulation has the same sequence as the apo A-I in Fig. 1A. However, in this case the amount of MdMD sampling time in the interval between examinations was increased from 60 fs to 600 fs and the force applied with the TCL-forces from each C_n to C_{n+7} (mapped onto the *XY*-plane) was lowered from the original 40 pN per pair to 20 pN per pair. These lowered parameters define our non-idealized system. In the case of POPC lipid bound apo A-I discoidal complex under these conditions has distortion from the planarity of the idealized model in Fig. 1A. Fig. 1B shows many conformational states observed in other thermal based MD studies and long-run dynamics simulations [36,37,47,48]. Interesting conformers were analyzed for energies from the entire archived trajectory (Fig. 5A). The mutant sequence has lower interaction energy between the two monomers at the Gly89/Ser188 and Glu107Cys mutation. The

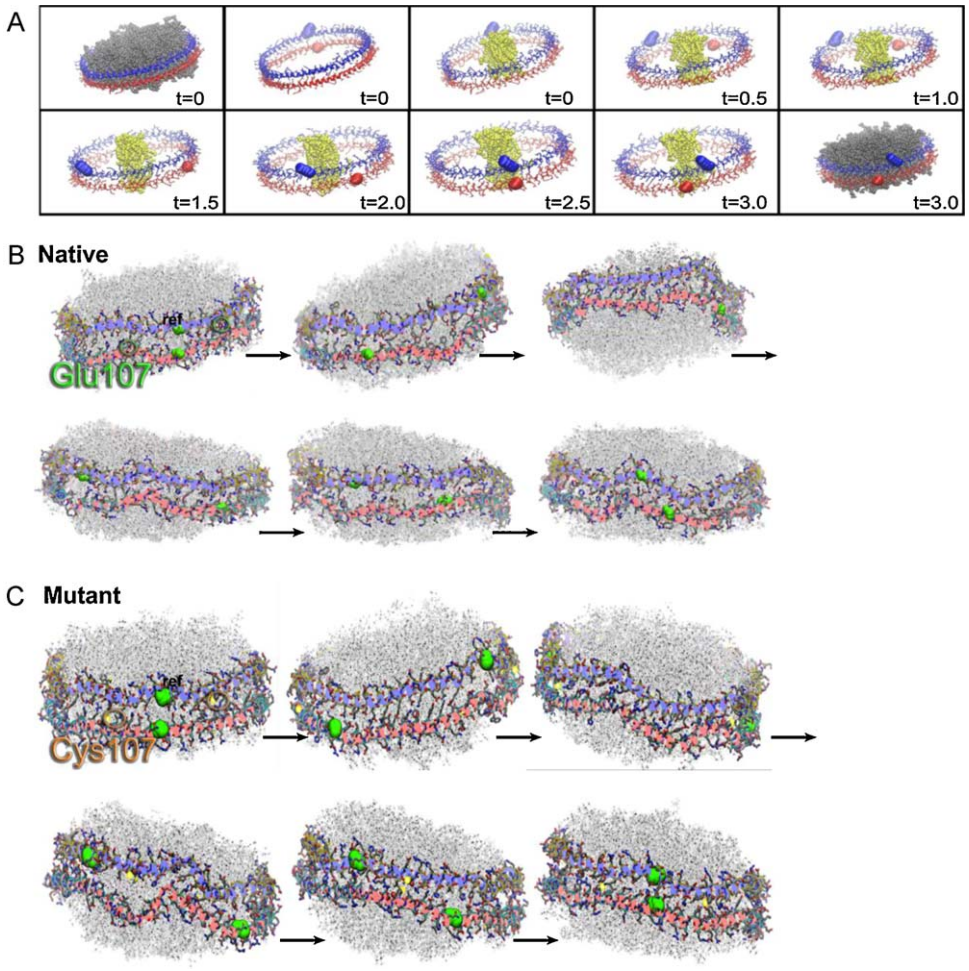

Fig. 1. Discoidal ApoA-I HDL particle inter-ring rotation using biased MdMD. (A) Idealized rotation of Apolipoprotein A-I driven along a circular path in *X*–*Y* plane, using by a biasing Tcl-forces script using NAMD2. This circular path is invoked with a 40 pN force vector pointed between the $C\alpha_n$ and $C\alpha_{n+7}$ atoms in the *X*–*Y* plane. The initial three panel shows $t = 0$ ns, where the lipids are only removed visually to allow for easier viewing. Lipids (176 POPC residues) are present during entire 3 ns. In the third panel on top, two ampipathic α-helical ApoA-I monomers (in red and blue) are rendered in licorice, while a small core of lipids (in yellow) illustrates overall stability during simulation. Using VdW rendering, enlarged residues (red and blue) clearly show the initial position of the two rings. The VdW residues highlight the pathway. (B) Non-idealized rotation of the native sequence for apolipoprotein A-I driven using biasing via MdMD Tcl-forces algorithm, which we implemented in NAMD2. This circular path is invoked with a 20 pN net force vector between $C\alpha_n$ and $C\alpha_{n+7}$ pairs. Which is projected onto the *X*–*Y* plane. A slow application of MdMD is applied biasing the sampling time. Non-perfect planarity of the protein monomers is achieved, while rotation continues as in the idealized case (A). Steps along the trajectory are shown with arrows separating different times in the pathway. (C) Non-idealized rotation of mutant (Glu107Cys) sequence for Apolipoprotein A-I driven using biasing via MdMD Tcl-forces algorithm, which we implemented in NAMD2. This circular path is invoked with a 20 pN net force vector between $C\alpha_n$ and $C\alpha_{n+7}$ pairs. Which is projected onto the *X*–*Y* plane. A slow application of MdMD is applied biasing the sampling time. Non-perfect planarity of the protein monomers is achieved, while rotation continues as in the idealized case (A). Steps along the trajectory are shown with arrows separating different times in the pathway

Gly88/Ser188 was not tested for a mutation simulation, but may bear repeating. The Glu107Cys mutation (purple line – Fig. 5A) is approximately 1 kcal/mol lower than in the native sequence (black line – Fig. 5A) at 2.5 ns MdMD run time. However, we note that there is also a lowered energy for the mutant at the Paris position around 1 ns of MdMD run time.

Fig. 1C is a continuous series of snapshots from both the native sequence and the mutant sequence of the discoidal apo A-I protein/POPC lipid complex (25 ns MdMD run time). A series of snapshots reveals the global conformational changes and 360° ring rotation as indicated by the reference molecule shown on each monomer as a large green sphere. The native sequence simulation has the same sequence as the apo A-I in Fig. 1A. However, for the much slower rate of rotation, our amount of MdMD sampling time is increased between 100 fs and 5000 fs for each demon scoring interval [45]. Also, the force applied with the TCL-forces at each C_n to C_{n+7} vector (mapped onto the *XY*-plane from the center of mass of the C_n) was lowered from the original 40 pN per pair to 20 pN per pair. These lowered parameters define our non-idealized system. In the case of POPC lipid bound apo A-I discoidal complex under these conditions has significant distortions from the planarity of the idealized model in Fig. 1A. Fig. 1C shows several conformational states observed in other thermal based MD studies and long-run dynamics simulations [36,37,47,48]. Interesting conformers were analyzed for energies from the entire archived trajectory (Fig. 5B).

Fig. 5C shows the mutant sequence has nominally lower interaction energy at the two monomers of the Gly89/Ser188 orientation. However, the mutant versus the native is nearly within twice the standard deviation, 0.256, at Gly89 or Ser188. However, the Milano paired conformation is significantly lower for the mutant than for the native sequence at a time of 4 ns MdMD run time. And the Paris position is worse for the mutant than the native sequence at a time of 7–8 ns of MdMD run time. Even more, the mutant is poor scoring for the Tyr126 paired orientation versus the native sequence with a difference in interaction energy of over 2 kcal/mol. Fig. 5B shows the Glu107 position is lower for the mutant but within the standard deviation for the longer amount of 23 ns MdMD run time.

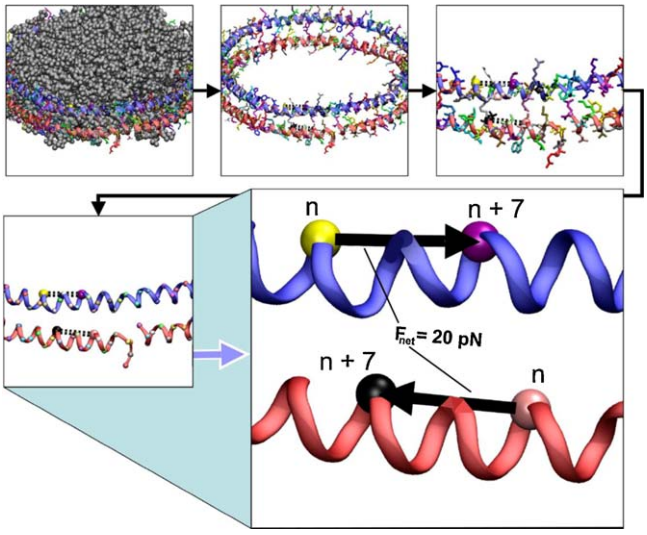

Fig. 2. Biasing scheme. Schematic for the apolipoprotein-AI Tcl-forces. Shown above on the left is the apolipoprotein-AI complex. The two protein ring monomers are colored red and blue to easily distinguish between them. The side chains are shown in licorice with a rainbow color scheme to distinguish residues. In the second panel, the lipids are not shown to reveal the shape of the two ring monomers. The third panel zooms in to reveal the alpha-helical shape and the interacting side chains. A dotted line shows the vector path of the force applied between n and $n+7$. The next panel simplifies this showing only Cα atoms and the alpha helix shape as a tube. The last panel zooms on two example pairs. The vectors applied to the two monomers A and B, the ampipathic α-helical proteins, are in opposite direction. The individual example force vector shown, $F = 10$ pN per C-alpha pair, is projected from the *XYZ* direction between n and $n+7$ onto the *X*–*Y* plane, which uses a 20 pN net force on both pairs above, or 10 pN per Calpha pair. Additional information on the MdMD biasing scheme is in Supplemental Fig. S2.

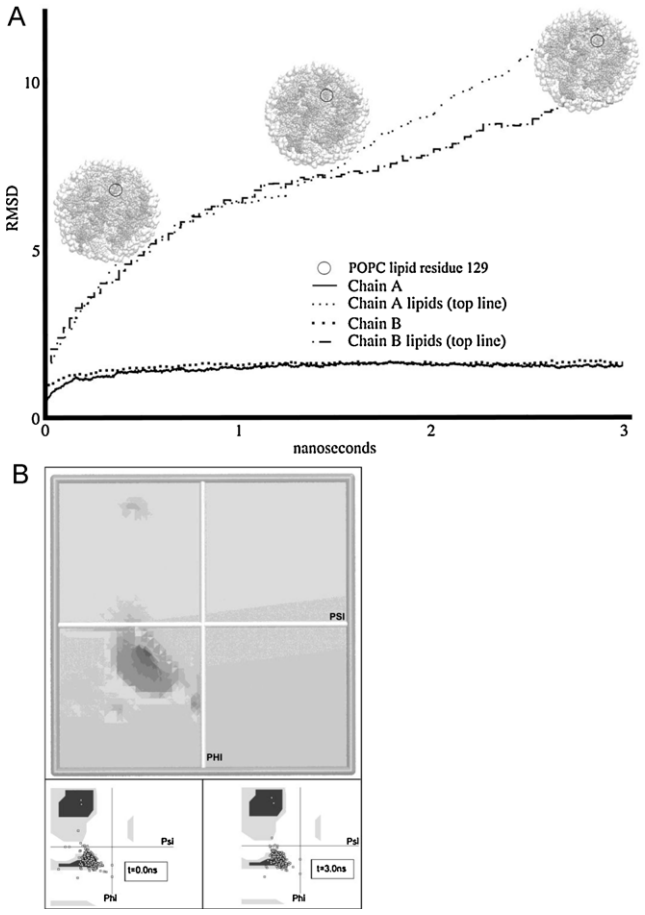

Fig. 3. RMSD and PHI/PSI plot. RMSD for the two molecules of the ampipathic α-helical ApoA-I monomers and the Phi/Psi space that the protein chains A and B during 3 ns simulation. (A) RMSD of ~2 Å for the two protein chains is show at the bottom of the graph. Shown in dotted and dot-dashed line above is the lipid RMSD for the 3 ns simulation. The unconfined lipid is free to move about; both lipid tails and headgroups RMSD grows from 3–10 Å. However, the overall POPC lipids are not deformed. The black circle shows the migration of POPC residue 129, which is fairly stable over the entire 3 ns trajectory. (B) Phi/Psi plots for the apolipoprotein-AI protein complex. The two protein ring monomers are shown in the contour map to illustrate the dominant α-helical character. The lower two Phi/Psi plots illustrate the α-helical character at the start and finish of the simulation. The two outliers on the upper left quadrant are the N- and C-terminal residues.

Supplemental Movie S2 and Movie S3 detail the MdMD-derived rotational motion for these systems.

It must be emphasized that a simulation of 3 ns with MdMD is not equivalent to 3 ns of MD. MdMD is only archiving successful steps as measured by the Maxwellian demon (Fig. S2). Incorrect, or bad steps, are discarded. With a success rate between 1% and 4%, and in some simulations under 1%, the total sampling time is large. For ring rotation of 3 ns, the true sampling time is approximately 300 ns. Slower rotational rate, with lower force, yields better success rates.

3.3. Ring rotation biasing

A schematic for the apo A-I biasing method using Tcl-forces is shown in Fig. 2. In the top left panel the original apolipoprotein-AI complex (protein – red and blue, lipids – gray). The model uses an α11/3 helical ring dimer that circumscribes an inner diameter of 85 Å and outer diameter of 105 Å. The 85 Å diameter patch consists of a 176 POPC bilayer. The second panel shows only the two protein ring monomers (red and blue) to reveal the shape of the two ring monomers. The side chains are shown in licorice (spectrum color scheme). The third panel zooms in to reveal the alpha-helical shape and the interacting side chains. A series of dotted lines in panel 3 show the approximate vector path for the force vector applied between residue n and residue $n+7$. The fourth panel simplifies the rendering by only showing the Cα atoms that are affected by the biasing force (α-helix shape shown as tubes). The fifth panel zooms on an example pair. The tcl-force biasing vector is visualized. The vector is applied to both of the two ampipathic α-helical ApoA-I monomers A and B, but in opposite direction. The bottom monomer illustrates the force vector ($F = 20$ pN), which is projected from the *XYZ* coordinates between n and $n+7$ onto an *X*–*Y* plane defined at the center of the apo A-I rings. The direction of the force applied is always in the n to $n+7$ direction with a force of 20 pN. For 203 residues, there are 29 force vectors for all Cα atoms in an *XY* plane. The amount of force was determined in an exhaustive series of simulations. Lower force resulted in unappreciable change in rotation, while larger forces derailed the monomer from the lipid bilayer (Supplemental Movie S4).

3.4. Implications for HDL structure

Fig. 3 depicts an analysis of the stability of the protein monomer-monomer *rings* and lipids during the 3 ns simulation for the idealized system shown in Fig. 1A. Fig. 3A shows the ampipathic α-helical ApoA-I monomers A and B are within 2.5 Å of their original conformation for the 3 ns simulation. This result abides well the biasing force with the required α-helical parameters required. Fig. 3B shows the top Phi–Psi plot places the α-helical parameters within the desired region. The large peak represents the sum of all Phi–Psi in that region. The average $\phi = -58^\circ$ and average $\varphi = -49^\circ$, which is consistent with an α11/3 helix. The two outliers we found at approximately $(-60^\circ, 75^\circ)$ were due to the N-terminus (1) and C-

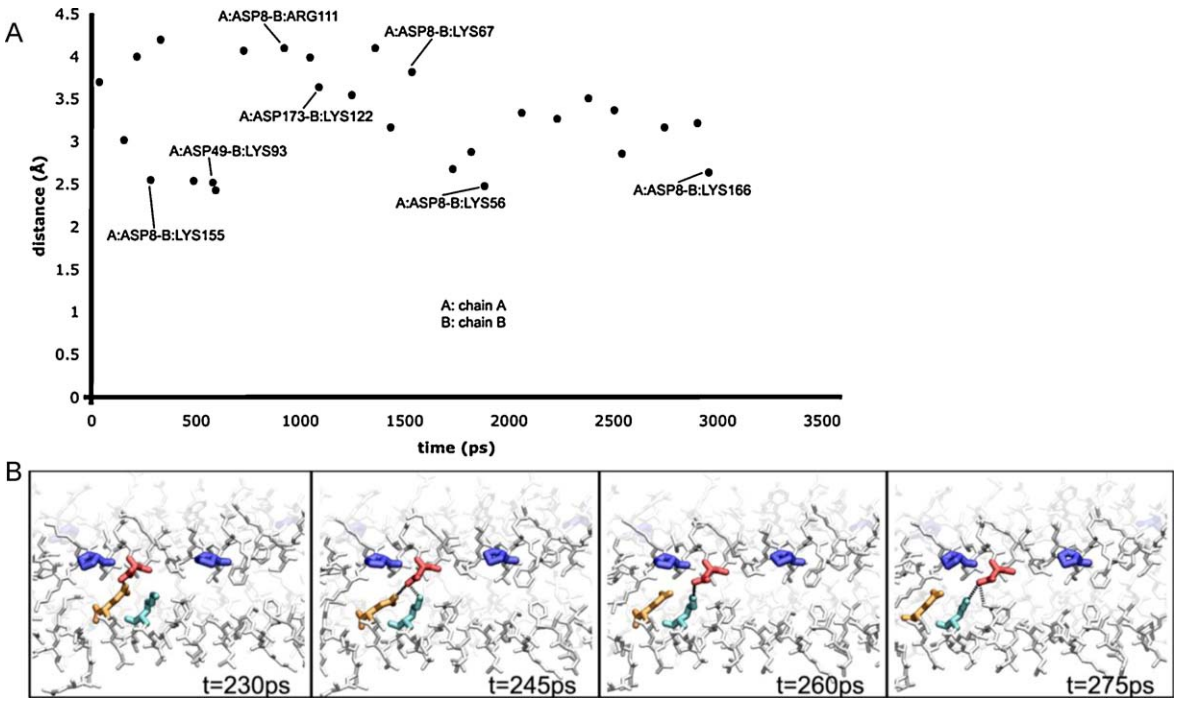

Fig. 4. Salt Walking, H-bond walking and representative salt bridge interactions. The ampipathic α-helical apo A-I protein monomers (chain A and B) undergo a 360° rotation during the course of the 3.5 ns MdMD run time. Time indicated in the panels is MdMD time. Over the course of this simulation time, intermolecular interactions form and break between chain A and chain B >165 times and between chain B and chain A >169 times. Salt bridges and hydrogen bond pairs formed in the side chain pairs between the two monomers formed and lost during the course of the simulation is >340. A salt bridge is defined as a distance-based interaction between the oxygen atom of the acidic residue and the nitrogen atom of the basic residue. The avg. length of the salt bridge was 3.35 Å with 95% of the salt bridges occurring between 2.77 Å and 3.93 Å. Bridges that formed between acidic monomers of chain A: ASP8, ASP49, ASP173, GLU30, GLU38, GLU45, GLU52, GLU70, GLU71, GLU85, GLU96, GLU107, GLU129, GLU143, GLU151, GLU158, GLU195 and basic monomers of chain B: ARG111, ARG133, ARG137, ARG151, ARG173, HSP115, HSP122, HSP159, LYS5, LYS19, LYS56, LYS67, LYS78, LYS93, LYS100, LYS155, LYS166, LYS199, and bridges formed between acidic monomers of chain B: ASP8, ASP49, ASP173, GLU30, GLU38, GLU45, GLU52, GLU70, GLU71, GLU85, GLU96, GLU107, GLU129, GLU143, GLU151, GLU158, GLU195 and basic monomers of chain A: ARG111, ARG133, ARG137, ARG151, ARG173, HSP115, HSP122, HSP159, LYS5, LYS19, LYS56, LYS67, LYS78, LYS93, LYS100, LYS155, LYS166, LYS199.

terminus (203) residue having a freer range of motion. The Phi–Psi plot at the bottom of Fig. 3B shows both the initial (t = 0 ns) and final conformation (t = 3 ns), indicating a stable protein structure throughout the simulation. Fig. 3A shows where the lipids have much more conformational searching. The POPC lipids range from 3 Å to around 10 Å RMSD over the 3 ns simulation. However, following one residue, POPC129 (shown in black circle), we observe that the relative position within the bilayer is unchanged. It has freedom to explore conformational space, but maintains position during simulation. Similar distributions for the Phi–Psi space were found amongst all models.

3.5. 'Salt Walking'

We measure all salt bridge interactions between acidic and basic residues from monomer A to monomer B and from monomer B to monomer A during the 3 ns simulation. We defined the criterion for the formation of a salt bridge when the interaction distance between the oxygen atoms of acidic residues and the nitrogen atoms of basic residues are within an average cut-off distance of 3.2 Å over the course of the trajectory timeline. The overall average salt bridge distance was found to be 3.35 Å with a standard deviation of 0.58. As measured by distance, 67% of measured salt bridges were within 2.77 Å and 3.39 Å. From protein monomer A to B, 165 salt bridges were formed and broken, while from protein monomer B to A, 169 salt bridges were formed and broken during the 3 ns simulation. A total of 334 salt bridges were formed and lost during the simulation.

Bridges that formed between acidic monomers of chain A: ASP8, ASP49, ASP173, GLU30, GLU38, GLU45, GLU52, GLU70, GLU71, GLU85, GLU96, GLU107, GLU129, GLU143, GLU151, GLU158, GLU195 and basic monomers of chain B: ARG111, ARG133, ARG137, ARG151, ARG173, HSP115, HSP122, HSP159, LYS5, LYS19, LYS56, LYS67, LYS78, LYS93, LYS100, LYS155, LYS166, LYS199, and bridges formed between acidic monomers of chain B: ASP8, ASP49, ASP173, GLU30, GLU38, GLU45, GLU52, GLU70, GLU71, GLU85, GLU96, GLU107, GLU129, GLU143, GLU151, GLU158, GLU195 and basic monomers of chain A: ARG111, ARG133, ARG137, ARG151, ARG173, HSP115, HSP122, HSP159, LYS5, LYS19, LYS56, LYS67, LYS78, LYS93, LYS100, LYS155, LYS166, LYS199. Lesser salt bridge interactions were not recorded.

In addition to measuring all salt bridge pairs (and hydrogen bond pairs), they were plotted over time (Fig. 4A). A representative plot shows the interaction pairs that form with the acidic residue, Aspartic acid 8, during the 3 ns simulation. As example, Asp8 from monomer A interacts with basic residues in chain B at Arginine111 (at t = 1 ns), Lysine67 (at t = 1.5 ns), Lysine56 (at t = 1.82 ns), and Lysine166 (at t = 3 ns). The plot in Fig. 4A shows the range of values from 2.5 to 4.2 Å in distance between possible salt bridge pairs. Fig. 4B shows a particular example: in panel 1, Aspartic acid 173 is in hydrogen bond formation with polar Gln203 at a distance of 3.18 Å (at t = 230 ps). In panel 2, over the next 15 ps, Asp173 partially breaks its hydrogen bond with Gln203 and forms a partial hydrogen bond to Lysine199. In panel 3, during the next 15 ps, Asp173 only maintains a bond to Lys199 at a distance of 2.68 Å (t = 260 ps). In panel 4, by t = 275 ps, Asp173 is losing its bond with Lys199 and moving to the next residue (Gln 195). In this way, the 'salt walking' and 'h-bond walking' progress along the X–Y plane in a circular path from one set of contact pairs to the next. We found similar salt walking properties among the other models. In addition, there are also helical openings that expose the side chains during rotation, which are discussed below.

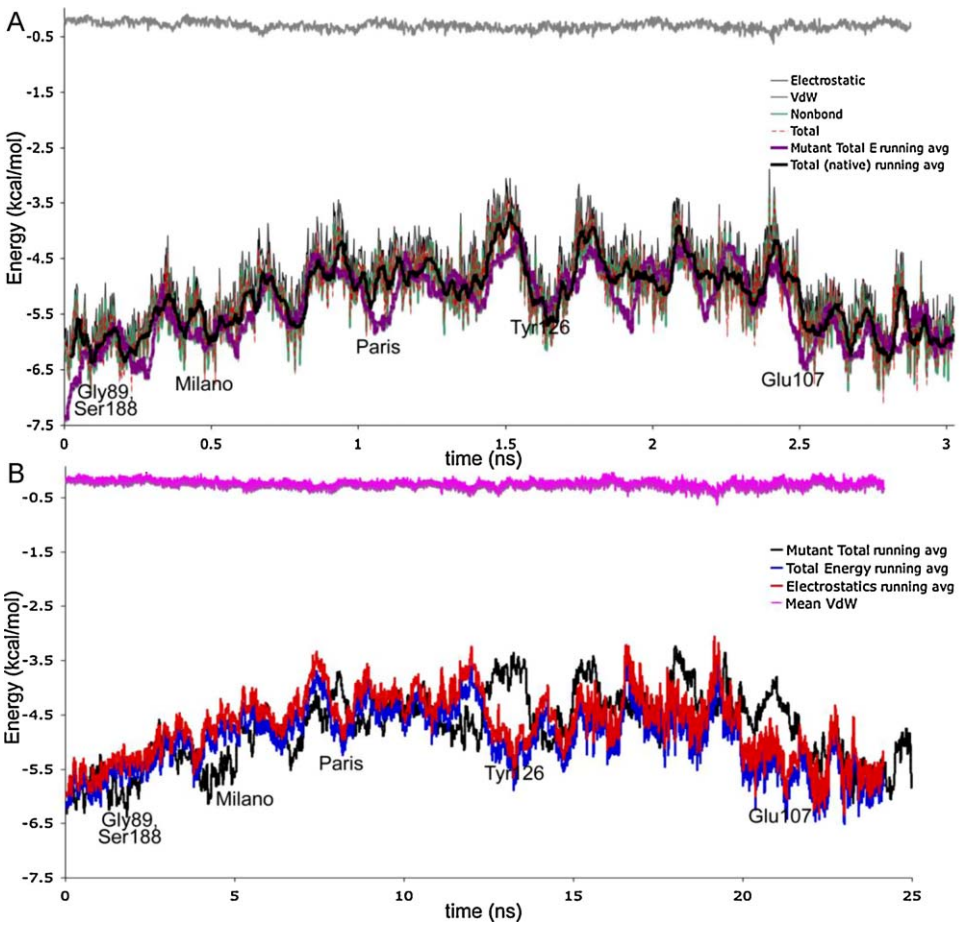

Fig. 5. Energies of stable conformers. Interaction energies for the two protein monomers of the ampipathic α-helical ApoA-I calculated over 3 ns of MdMD run time (300 ns sample time) and 30 ns MdMD run time (~800 ns sample time). (A) The graph illustrates the energy output for the 3 ns MdMD run time, corresponding to ~300 ns of MD sampling time. The Paris (R173C) and Milano (R151C) mutation locations occur at time = 0.5 ns MdMD run time and 1.2 ns MdMD run time, respectively. Tyr126 exhibits similar energetic properties at time = 1.72 ns. Improved energetic conformations were observed at Ser184 (t = 0.15 ns MdMD run time), Glu107 (t = 2.52 ns MdMD run time). The energies spread over all 406 residues amongst the two monomers of 203 apiece, accounts for around 4.5 and 7.5 kcal/mol, slightly above the nominal thermal barriers. (B) The graph illustrates the energy output of the 25 ns MdMD run time, corresponding to ~800 ns of MD sampling time. The Paris (R173C) and Milano (R151C) mutation locations occur at time = 5 ns MdMD run time and 8.5 ns MdMD run time, respectively. Tyr126 exhibits similar energetic properties at time = 14.5 ns. Improved energetic conformations were observed at Ser184 (t = 2.0 ns MdMD run time), Glu107 (t = 21 ns MdMD run time). The energies spread over all 406 residues amongst the two monomers of 203 apiece, accounts for around 4.5 and 6.5 kcal/mol, slightly above the nominal thermal barriers.

3.6. Conformational analysis

Fig. 5A shows the energies for several simulations plotted for their interaction energies between the two protein monomers of lipid-bound apo A-I discoidal complex. The total energy and interaction energy are composites of the electrostatic and VdW energies, since those are the two dominant energy contributors. The VdW contribution was nominal and is indicated to be only 20% of the total energy. The low peaks indicate the stable conformations, which are a result of strong salt bridge interaction. Indicated in Supplemental Fig. S1, the Paris and Milan mutations are a two of the lower peaks. Examining the energetics on a per residue basis yields, the Paris (R151C registration) occurring at time = 1.13 ns with an $E = -3.73$ kcal/mol, and the Milano (R173C) occurred at time = 0.488 ns and $E = -4.22$ kcal/mol. However, these are not the lowest energetic conformations revealed from the simulation. Three additional conformations were observed to have lower energies. Using registration nomenclature, Serine184 is aligned in both monomer A and B at t = 0.1–0.15 ns, where the energy is −4.92 kcal/mol. Tyr has an energy of −3.82 kcal/mol at t = 1.92 ns. Glu107 has an energy of −5.67 kcal/mol at t = 2.52 ns. Interestingly, Gly89–Gly89 and Ser188–Ser188 self aligns twice during the simulation: first at t = 0 ns with the $E = -6.26$ kcal/mol, and second at t = 2.82 ns with $E = -4.87$ kcal/mol. We do not suggest Ser184, Gly89, Ser188, or Glu107 are most favorable residues for Cys mutations to occur, but rather these registrations seem to have an optimal salt bridge score (see Section 3). For the sake of experimental clarity, we did examine a Glu107Cys mutant for any energetic differences from the native sequence. There is some indication that the cysteine mutant is more favorable. The results for this are shown in Fig. 5A and B and discussed above.

Additionally, the effect of the rotational motion on the side chains inter-protein interactions are not necessarily completely duplicated upon a subsequent rotations, while rotation puts limits on side chain sampling time during intervals of interaction. The rotational effect is lessened over longer rotation times than in shorter sampling runs; see a comparison of the energy profile in Fig. 5A and B.

4. Conclusions

Previously, preferred conformations of the two alpha-helical monomers was based on salt bridge scoring for various alignments [14]; which demonstrated preferred *energy* scoring of specific registrations, e.g. the L5/5, Milano mutant, or Paris mutant [15]. The previous salt bridge scoring data supported a double belt model and X-ray crystal structure observed [9,13]. Additionally, the impor-

tant Paris and Milano mutants form a disulfide bridge at residues 151 and 173, respectively. The Paris and Milano mutants indicate a mode of change must be available to find proper registration. One proposed change is a rotationally circular motion of the protein monomers about the unilamellar bilayer contained within the core. The mutants that possess cysteine in place of the arginine residue can lock the lipoprotein into a fixed conformation.

The simulation presented here supports the existing double-belt model. The salt bridge patterns found in the *salt walking* data suggest a method for conformational switching during discoidal formation of apolipoprotein A-I HDL. The data reflects a geometric sliding relationship along the edge of the POPC lipid bilayer that allows for the protein to accommodate for the influx of additional POPC lipids. This lateral mode of sliding would allow for the registration of the two ampipathic α-helix protein chains to alter significantly allowing Milano and Paris mutants to search for the registration that allows the cysteine mutants to form a disulfide bond. Two remarkable features of this simulation and generated models are: the well-maintained interhelical geometry and favorable energetic scoring indicating alternate conformations. The wild-type does not maintain the lowest salt bridge score throughout the simulation. In the idealized model, the wild type conformation occurs at $t = 0$ ns and $t = 2.82$ ns. By 2.82 ns, the score is no more favorable than that of Paris or Milano mutant registration. The lowest score is for Glu107–Glu107 registration. It is well known that the Paris and Milano mutations are exactly 22 residues apart in the sequence. Interestingly, Glu107 is positioned exactly two 22-mers from the Paris Mutant (R151) and three 22-mers from the Milano mutant (R173). The abundance of salt bridges observed for the Milano mutant and Paris mutant conformations are particularly favorable [14,20,24], and this is one reason for the low energy observed by the stabilizing presence of the abundance of salt bridges. Likewise, we find for Glu107 that there is an abundance of salt bridges that lowers the energy significantly (Fig. 5). Also, the wild type shown in previous salt bridge scoring metrics is considered very favorable [15]. But, after 3 ns of simulation and over a 400° rotation of the two protein monomers, there is a suggestion that the wild type is not more favorable than the Paris or Milan mutants (Fig. 5). Without an uphill energetic cost, it is plausible that the conformational switch from wild type to the Paris or Milano mutation is not insurmountable. Likewise, Glu107 seems to be energetically favorable by comparison when examining either the idealized model or non-planar models.

Fig. 1C and Supplemental Movie S3 show the opening between monomers of the alpha helices that form the discoidal complex of lipid-bound apo A-I. In these instances, the rotational motion contributes to release of the salt bridges, temporary interaction with the solvent, and lateral motion allowing new salt bridges to form. The slower rotating systems have more solvent exposure time, whereas the quickly rotating idealized system moved too quick for out-of-plane deformation and solvent disruptions. It appears that solvent disruptions may play a key role in allowing the two monomers to release from interaction and find new pairings.

Fig. 5A scoring of low energy conformations may be useful for determining experimental tests of mutants. Similarities between the Milano and Paris mutant apo A-I salt bridge scoring, the 22-mer periodicity, and energetic scoring shown in Supplemental Fig. S1 predicts that Glu107 could be used to generate a viable mutant. The substitution of a cysteine residue for glutamic acid 107 should generate a mutant with similar structural and functional properties to the Paris and Milano apo A-I mutants. Fig. 5B does not demonstrate the same energy profile for the mutant although the native sequence is similar. The slower rate or rotation and longer sampling time allowed other more opportunistic interactions to dominate side chain interactions. And, there were much more substantial inter-helical disruptions allowing solvent to participate during rotation than in the native sequence case (Supplemental Movie S3). And, there are indications from the mutant simulation that reaffirms the strength of the Milano mutant. However, at the MdMD run time of 3 ns (300 ns MD sampling time), there seems to be confirmation of the Glu107Cys mutant. Interest in experimentally testing the Glu107Cys mutant may be worthwhile, given the indication of it's strong interaction.

Also noteworthy is the recent work of Segrest and co-workers coarse-grained approach on formation of spherical particles starting from discoidal models [48]. One area that could be additionally explored is the failure for the spherical-type particles to form in the case of the disulfide bridge with the Paris and Milano mutants, and with the proposed mutants here.

Acknowledgements

We thank Drs. Jere P. Segrest and Stephen C. Harvey for sharing their models of the apolipoprotein A-I and useful discussions on this topic. Additionally, we thank Dr. Anton Petrov simulation discussions.

Appendix A. Supplementary data

Supplementary data associated with this article can be found, in the online version, at doi:10.1016/j.jmgm.2011.04.005.

References

[1] J.P. Segrest, R.L. Jackson, J.D. Morrisett, A.M. Gotto Jr., A molecular theory of lipid–protein interactions in the plasma lipoproteins, FEBS Lett. 38 (1974) 247–253.
[2] D. Atkinson, M.A. Davis, R.B. Leslie, The structure of a high density lipoprotein (HDL3) from porcine plasma, Proc. Natl. Acad. Sci. U.S.A. 186 (1974) 165–180.
[3] C.G. Brouillette, G.M. Anantharamaiah, Structural models of human apolipoprotein A-I, Biochim. Biophys. Acta 1256 (1995) 103–129.
[4] E. Aakerloef, H. Joernvall, H. Slotte, A. Pousette, Identification of apolipoprotein-A1 and immunoglobulin as components of a serum complex that mediates activation of human sperm motility, Biochemistry 30 (1991) 8986–8990.
[5] W. Zhou, M.M. Ross, A. Tessitore, D. Ornstein, A. Vanmeter, L.A. Liotta, et al., An initial characterization of the serum phosphoproteome, Proteome Res. 8 (2009) 5523–5531.
[6] W.P.R. Castelli, P.W.F. Garrison, R.D. Wilson, S.K. Abbott, W.B. Kannel, Incidence of coronary heart disease and lipoprotein cholesterol levels, J. Am. Med. Assoc. 256 (1986) 2835–2838.
[7] G.J. Miller, N.E. Miller, Plasma-high-density-lipoprotein concentration and development of ischaemic heart disease, Lancet i (1975).
[8] N.E. Miller, D.S. Thelle, O.H. Fördé, O.D. Mjös, The Tromso Heart Study: high-density lipoprotein and coronary heart disease: a prospective case–control study, Lancet i (1977).
[9] A. Wlodawer, J.P. Segrest, B.H. Chung, R. Chiovetti Jr, J.N. Weinstein, High-density lipoprotein recombinants: evidence for a bicycle tire micelle structure obtained by neutron scattering and electron microscopy, FEBS Lett. 104 (1979) 231–235.
[10] D. Atkinson, D.M. Small, G.G. Shipley, X-ray and neutron scattering studies of plasma lipoproteins, Ann. N.Y. Acad. Sci. 348 (1980) 284–298.
[11] A. Jonas, J.H. Wald, K.L. Toohill, E.S. Krul, K.E. Kezdy, Apolipoprotein A-I structure and lipid properties in homogeneous, reconstituted spherical and discoidal high density lipoproteins, J. Biol. Chem. 265 (1990) 22123–22129.
[12] D.M. Monti, F. Guglielmi, M. Monti, F. Cozzolino, S. Torrassa, A. Relini, et al., Effects of a lipid environment on the fibrillogenic pathway of the N-terminal polypeptide of human apolipoprotein A-I, responsible for in vivo amyloid fibril formation, Eur. Biophys. J. 39 (2009) 1289–1299.
[13] D.W. Borhani, D.P. Rogers, J.A. Engler, C.G. Brouillette, Crystal structure of truncated human apolipoprotein A-I suggests a lipid-bound conformation, Proc. Natl. Acad. Sci. U.S.A. 94 (1997) 12285–12290.
[14] J.P. Segrest, M.K. Jones, A.E. Klon, C.J. Sheldahl, M. Hellinger, H. De Loof, et al., A detailed molecular belt model for apolipoprotein A-I in discoidal high density lipoprotein, J. Biol. Chem. 274 (1999) 31755–31758.
[15] A.E. Klon, M.K. Jones, J.P. Segrest, S.C. HArvey, Molecular belt models for the apolipoprotein A-I Paris and Milano mutations, Biophys. J. 79 (2000) 1679–1685.
[16] C.J. Sheldahl, S.C. Harvey, Molecular dynamics on a model for nascent high-density lipoprotein: role of salt bridges, Biophys. J. 76 (1999) 1190–1198.
[17] H. Heller, M. Schaefer, K. Schulten, Molecular dynamics simulation of a bilayer of 200 lipids in the gel and in the liquid-crystal phases, J. Chem. Phys. 97 (1993) 8843–9360.

[18] M.N. Palgunachari, V.K. Mishra, S. Lund-Katz, M.C. Phillips, S.O. Adeyeye, S. Alluri, et al., Only the two end helixes of eight tandem amphipathic helical domains of human Apo A-I have significant lipid affinity: implications for hdl assembly, Arterioscl. Thromb. Vascul. Biol. 16 (1996) 328–338.
[19] V.K. Mishra, M.N. Palgunachari, Interaction of model class A1, class A2, and class Y amphipathic helical peptides with membranes, Biochemistry 35 (1996) 11210–11220.
[20] M.K. Jones, G.M. Anantharamaiah, J.P. Segrest, Computer programs to identify and classify amphipathic alpha helical domains, J. Lipid Res. (1992) 287–296.
[21] J.P. Segrest, H. De Loof, J.G. Dohlman, C.G. Brouillette, G.M. Anantharamaiah, Amphipathic helix motif: classes and properties, Proteins 8 (1990) 103–117.
[22] K.H. Weisgraber, J.S.C. Rall, T.P. Bersot, R.W. Mahley, G. Franceschini, C.R. Sirtori, Apolipoprotein A-I (Milano), J. Biol. Chem. 258 (1983) 2508–2513.
[23] E.A. Bruckert, E.H. Funke, I. Beucler, H. Wiebusch, G. Turpin, G. Assmann, The replacement of arginine by cysteine at residue 151 in apolipoprotein A-I Milano produces a phenotype similar to that of apolipoprotein A-I, Arterioscl. Thromb. Vascul. Biol. 128 (1997) 121–128.
[24] A.G. Rocco, L. Mollica, E. Gianazza, L. Calabresi, G. Franceschini, C.R. Sirtori, et al., Model structure for the heterodimer apoA-IMilano–apoA-II supports its peculiar susceptibility to proteolysis, Biophys. J. 91 (2006) 3043–3049.
[25] L.G. Calabresi, A. Franceschi, A. Burkybile, A. Jonas, Activation of lecithin cholesterol acyltransferase by a disulfide-linked apolipoprotein A-I dimer, Biochem. Biophys. Res. Commun. 232 (1997) 345–349.
[26] G. Franceschini, L.G. Calabresi, G. Chiesa, C. Parolini, C.R. Sirtori, M. Canavesi, et al., Increased cholesterol efflux potential of sera from ApoA-I(Milano) carriers and transgenic mice, J. Clin. Investig. 66 (1999) 892–900.
[27] U. Daum, C. Lanager, N. Duverger, F. Emmanuel, P. Benoit, P. Denefle, et al., Apolipoprotein A-I(R151C)Paris is defective in activation of lecithin: cholesterol acyltransferase but not in initial lipid binding, formation of reconstituted lipoproteins, or promotion of cholesterol efflux, J. Mol. Med. (1999) 77.
[28] M. Pérusse, A. Pascot, J.P. Després, C. Couillard, B. Lamarche, A new method for HDL particle sizing by polyacrylamide gradient gel electrophoresis using whole plasma, J. Lipid Res. 42 (2001) 1331–1334.
[29] A.E. Klon, J.P. Segrest, S.C. Harvey, Comparative models for human apolipoprotein a-I bound to lipid in discoidal high-density lipoprotein particles, Biochemistry 41 (2002) 10895–10905.
[30] Accelrys, I. Accelrys Inc., 9685 Scranton Road, San Diego, California 92121, USA. amaiti@accelrys.com. INSIGHT-II. 2000.
[31] W. Humphrey, A. Dalke, K. Schulten, VMD: visual molecular dynamics, J. Mol. Graph. 14 (33–8) (1996) 27–28.
[32] J.P. Krawetz, A. Shinozaki, K. Varadarajan, K. Schulten, NAMD2: greater scalability for parallel molecular dynamics, J. Comput. Phys. 151 (1999) 283–312.
[33] M. Nelson, W. Humphrey, A. Gursoy, A. Dalke, L. Kalé, R.D. Skeel, et al., NAMD—a parallel object-oriented molecular dynamics program, J. Supercomput. Appl. 10 (1996) 251–268.
[34] M.K. Jones, A. Catte, L. Li, J.P. Segrest, Dynamics of lecithin:cholesterol acyltransferase activation by apolipoprotein A-I, Biochemistry 48 (2009) 11196.
[35] A.E. Klon, M.K. Jones, J.P. Segrest, S.C. Harvey, Molecular belt models for the apolipoprotein A-I Paris and Milano mutations, Biophys. J. 79 (2000) 1679–1685.
[36] M.K. Jones, A. Catte, J.C. Patterson, F. Gu, J. Chen, L. Li, et al., Thermal stability of apolipoprotein A-I in high-density lipoproteins by molecular dynamics 96 (2) (2009) 354–371.
[37] A. Catte, J.C. Patterson, M.K. Jones, W.G. Jerome, D. Bashtovyy, Z. Su, et al., Novel changes in discoidal high density lipoprotein morphology: a molecular dynamics study, Biophys. J. 90 (2006) 4345–4360.
[38] W.L. Jorgensen, J. Chandrasekhar, J.D. Madura, R.W. Impey, M.L. Klein, Comparison of simple potential functions for simulating liquid water, J. Chem. Phys. 79 (1983) 926–935.
[39] B.R. Brooks, R.E.B. Olafson, D.J. States, S. Swaminathan, M. Karplus, CHARMM: a program for macromolecular energy, minimization, and dynamics calculations, J. Comput. Chem. 4 (1983) 187–217.
[40] J. Ryckaert, G. Ciccotti, H. Berendsen, SHAKE: numerical integration of the cartesian equations of motion of a system with constraints: molecular dynamics of n-alkanes, J. Comput. Phys. 23 (1977) 327–341.
[41] T. Darden, D. York, L. Pedersen, Paticle Mesh Ewald—an N. Log(N) method for Ewald sums in large systems, J. Chem. Phys. 98 (1993) 10089–10092.
[42] E. Nosé, A unified formulation of the constant temperature molecular dynamics method, J. Chem. Phys. 81 (1984) 511–519.
[43] W.G. Hooover, Canonical dynamics: equilibrium phase-space distributions, Phys. Rev. A 31 (1985) 1695–1697.
[44] H.J.C. Berendsen, J. Postma, W. Van Gunsteren, A. Dinola, J. Haak, Molecular-dynamics with coupling to an external bath, J. Chem. Phys. 81 (1984) 3684–3690.
[45] T. Caulfield, B. Devkota, G. Rollins, Examinations of tRNA range of motion using simulations of cryo-EM microscopy and X-ray data, J. Biophys. 2011 (2011), doi:10.1155/2011/219515.
[46] S.C. Harvey, H.A. Gabb, Conformational transitions using molecular dynamics with minimum biasing, Biopolymers 33 (1993) 1167–1172.
[47] F. Gu, M.K. Jones, J. Chen, J.C. Patterson, A. Catte, W.G. Jerome, et al., Structures of discoidal high density lipoproteins: a combined computational-experimental approach, J. Biol. Chem. 285 (2010) 4652–4665.
[48] A. Catte, J.C. Patterson, D. Bashtovyy, M.K. Jones, F. Gu, L. Li, et al., Structure of spheroidal HDL particles revealed by combined atomistic and coarse-grained simulation, Biophys. J. 94 (2008) 2306.